Field emission at nanometer distances for high-resolution positioning

A. J. le Fèbre,[a] L. Abelmann, and J. C. Lodder
MESA + Institute for Nanotechnology, P.O. Box 217, 7500 AE Enschede, Netherlands

(Received 4 September 2007; accepted 14 February 2008; published 1 April 2008)

The dependence of the field emission effect on distance is applied for displacement sensing and high-resolution positioning. Silicon atomic force microscopy probes were used as a field emission source by applying voltages up to 400 V between this probe and a counter-electrode sample consisting of TiW sputtered on a silicon wafer. From current-voltage characteristics measured for distances varying from 50 to 950 nm, values for the field enhancement factor were determined which show a dependence on the electrode separation. This dependence can be correctly described by a model the authors developed using finite-element calculations and is determined by the emitter geometry and tip radius. Feedback to the probe position was used to maintain a constant current to apply this distance dependence for positioning. When increasing the applied voltage from 5 to 40 V for a constant current of 3 nA, the probe position is raised ~90 nm. The nonlinear sensitivity of this positioning method is determined by the varying field enhancement and can be fitted by the same calculated model. Using feedback, the field emitter can be positioned with high lateral resolution and scanned over a conducting surface. Increasing the bias voltage from 3 to 50 V results in an increase in the emitter-sample distance and a decrease in lateral resolution. Damage to the scanned surface has to be prevented by using a current-limiting resistor and by annealing the probe and sample under ultra high vacuum conditions before use. © *2008 American Vacuum Society.*
[DOI: 10.1116/1.2894898]

I. INTRODUCTION

Field emission studies are often conducted with several millimeters distance between the field emitter and counter-electrode, so that the electric field is less sensitive to variations in the initial distance. For most measurements this is important, since the emission properties of a certain emitter are to be investigated regardless of distance. At small separations, however, the turn-on voltage that is needed to achieve a certain emission current becomes very sensitive to the separation distance, depending on the specific electrode configuration.[1] This strong dependence greatly complicates the understanding of experimental data when the distance between field emitter and counter-electrode and the field emitter geometry are not exactly known. Therefore, it is important to know how these factors affect the measurements and what initial distance is needed to minimize the effect.

On the other hand, when the field emitter and counter-electrode are deliberately brought close together, the distance dependence of the field emission effect can be applied as a displacement sensing method.[2] Such a displacement sensor could be used in the field of nanoelectromechanical systems (NEMS), where sensors are needed with a critical sensing area in the nanometer range, with sufficient sensitivity and signal-to-noise ratio. We will present measurement results on this displacement sensing method which uses the distance dependence of the field emission effect. Our aim is to apply this sensing method in a magnetic probe storage system.[3] Such a system is expected to give a promising route toward extremely high density recording, by scanning an array of sharp probes relative to a storage medium to write and read data.[4] In *magnetic* probe storage, there is a need to position individual probes at several nanometers above the recording medium. Therefore, in this work, we present measurement results on a novel concept using field emission currents for high resolution positioning at nanometer distances.

II. MODEL CALCULATION FOR THE DISTANCE DEPENDENCE OF FIELD ENHANCEMENT

To include the distance dependence of the field emission current in the standard Fowler-Nordheim theory, here we follow the formulation and parameter conventions as used in a recent treatment given by Forbes:[5]

$$I = t^{-2}(y)\frac{aA}{\phi}E^2(d)\exp\left\{v(y)\frac{-b\phi^{3/2}}{E(d)}\right\} \quad \text{(A)}. \tag{1}$$

In this equation $E(d)$ is the electric field which depends on distance d between field emitter and electrode, ϕ is the work function, A is the area of emission, and a and b are universal constants given by $a=1.54\times10^{-6}$(A eV V^{-2}) and $b=6.83\times10^{9}$(eV$^{-3/2}$ V m^{-1}). The functions $t(y)$ and $v(y)$ are the mathematical correction functions which are introduced to include the Schottky dependence of the image-rounded potential barrier shape, with $y=((e^3/4\pi\epsilon_0)E)^{1/2}/\phi$ (Ref. 6).

Since the electric field is proportional to the applied voltage and the emitter-sample distance, the field emission current signal can be used for displacement sensing. When using field emitter tips, the emission current is determined by the *local* electrical field close to the apex of the emitting tip. This local electric field is often significantly higher than the electric field for a parallel plate configuration, and the ratio of these fields is given by the *field enhancement factor* γ.[7] In the geometrical configuration of a tip and flat electrode, the

[a]Electronic mail: a.j.lefebre@utwente.nl

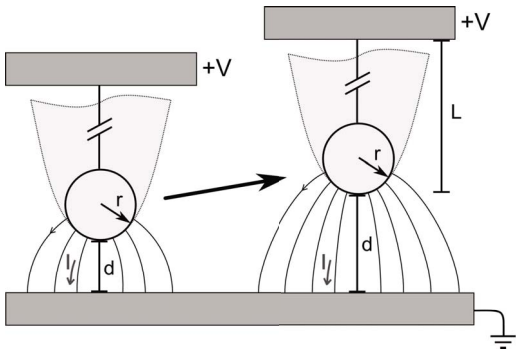

FIG. 1. Geometric model and symbol definitions used for calculating the field enhancement factor for an emitter tip of length L with radius r, at distance d from the counter-electrode.

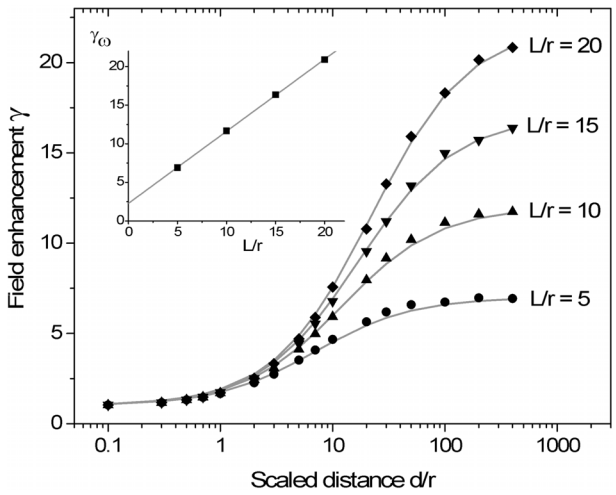

FIG. 2. Field enhancement factors as function of distance determined by FEM calculation for increasing tip lengths $L=5r$, $L=10r$, $L=15r$, and $L=20r$. The inset shows the corresponding maximum field enhancement factors at large distance.

maximum electric field E_{local} at the tip end is defined by

$$E_{local}(d) = \gamma(d)\frac{V}{d}, \tag{2}$$

where V is the voltage across a gap of thickness d. Since the field enhancement factor γ is determined by the geometry, it also depends on the separation distance d and is therefore of particular interest if we want to determine the dependence of the field emission current on distance.

Different approaches for the derivation of this field enhancement factor can be found in the literature.[1,7–10] Generally, it is assumed that the distance between the field emitter tip apex and the counter-electrode can be neglected, since it is much larger than the tip radius and the length of the field emitter. However, at small separations this assumption is not valid and a model to estimate the field enhancement for small distance is needed.

To find an expression describing the distance dependence of the field enhancement factor, we assume that the emitter and sample surfaces are at fixed potentials, which reduces the problem to solving Laplace's equation for a given applied voltage and distance between the tip and sample. To further simplify the problem, the emitter-sample geometry is approximated by a sphere in between a parallel plate configuration.[7] See Fig. 1 for an illustration and definition of the parameters used. Here the emitter tip end is represented by a sphere at uniform potential, connected to the top electrode, while the bottom electrode is at ground potential. Although this geometry approximation is probably not valid for the complicated emitter shape that we utilize in our experiments, this simple model is used to study the effect of tip radius and tip-electrode distance on the field enhancement.

The enhancement factor γ for this configuration was calculated by finite element method (FEM) with FREEFEM^{++} software software,[11] using the Laplace equation in cylindrical coordinates in weak form representation.[12] Since the electric potential changes rapidly at the apex of the sphere, a very high density of finite element nodes is needed at this point to obtain an accurate solution. The repeated use of the adaptmesh function was used to generate a mesh with high density in this region. The size of the calculated geometry and the number of mesh refining iterations was increased until the relative error between two subsequent calculations was less then 10^{-3}.

From the FEM calculations, the value of the electric field was determined at the apex of the sphere, closest to the counter-electrode. By dividing this value by the planar electric field V/d the field enhancement factor is obtained. In Fig. 2 the FEM results for this field enhancement factor are plotted as function of the scaled distance d/r and can be approximated by the following relation:

$$\gamma(d) = \frac{\gamma_\infty(r+d)}{\gamma_\infty r + d}, \tag{3}$$

which describes the field enhancement at the apex of a sphere with radius r at a distance d from a flat counter-electrode, with γ_∞ the field enhancement at large distance. Although this relation does not perfectly fit the FEM results, it is in good agreement with our expectations for the distance dependence of the field enhancement factor: for small distance ($d \leq r$), the electrode configuration approaches a parallel plate configuration ($\gamma \simeq 1$); for increasing distance, the field enhancement factor rises rapidly; and for large distance ($d > 100r$) it saturates to a maximum value ($\gamma = \gamma_\infty$). When this result is compared to an often mentioned model presented by Miller,[10] giving the distance dependence by the formula $\gamma(d) = \gamma_\infty d/(d+L)$, it is found that for larger distances the results overlap. However, for small separations, Miller's equation suggests that γ approaches zero as d becomes very small, whereas it should approach unity as in the result of Eq. (3). The influence of the emitter tip length L was determined by repeating the FEM calculations for increasing L. From these calculations the value for the maximum field enhancement was found to saturate to

$$\gamma_\infty = L/r + m, \tag{4}$$

with $m=2.5$, which is in agreement with analytical results obtained by others.[7]

III. EXPERIMENT SETUP AND SAMPLES

A UHV scanning probe microscope was used to measure field emission characteristics as a function of distance and for high-resolution positioning. The microscope scanner was used to approach individual field emitter probes to a conductive sample that acts as a counter-electrode. The sample could be scanned by applying scan voltages to the three scan piezos for XY-scans with 5×5 μm^2 range and to the center piezo for Z-positioning of the probe with 1 μm range. The UHV system is operated at 5×10^{-9} mbar. Further details on the measurement setup have been described previously.[3]

As field emitters we used the tips of commercially available atomic force microscopy (AFM) probes (Nanosensors PPP-NCLR). This single crystal silicon probe, n-type doped with a level of 5×10^{18} atoms/cm^3(<0.01 Ω cm), has a tip height of $10-15$ μm and a radius of typically <7 nm. Previous measurements showed that the probe cantilever deflection is limited to <10 nm due to its high force constant (48 N/m).[13] For the following results we will therefore assume that the deflection is negligible.

For the first characterization measurements of the field emitter probes we used a flat silicon wafer sample sputtered with 86 nm TiW to act as a counter-electrode. For the subsequent measurements using field emission currents for high-resolution lateral positioning, special patterned samples were prepared by laser interference lithography, resulting in nanodots of 365 nm periodicity, 190 nm diameter, and 35 nm height. A 20 nm metal coating (Cr/Pt) was sputtered on the patterned layer to make the samples conductive.[3]

IV. RESULTS AND DISCUSSION

A. Field emission from AFM probes at small distances

Measurements of the distance dependence of the field emission I/V characteristics are shown in Fig. 3(a). Here the AFM probe was first brought into the tunneling regime, so close to contact with the flat TiW coated sample. Next the probe was retracted to increase the probe-sample distance to a fixed value. A positive bias sweep was then applied to the sample to extract current from the probe tip. This measurement was repeated for increasing probe-sample distances from 50 to 950 nm. In Fig. 3(b), the corresponding Fowler-Nordheim (FN) plots are given.

By fitting the FN plots the typical parameters for the Fowler-Nordheim equation can be obtained, i.e., the emission area and the field enhancement factor. For this an automated fitting routine was developed in the mathematical package MAPLE™, based on the model described in Ref. 5. For the work function we used the value for intrinsic silicon $\phi=4.95$ eV (Ref. 14) and the correction factors were calculated using the elliptic-integral formulas given in Ref. 6. It should be noted that since the correction factors $t(y)$ and $v(y)$

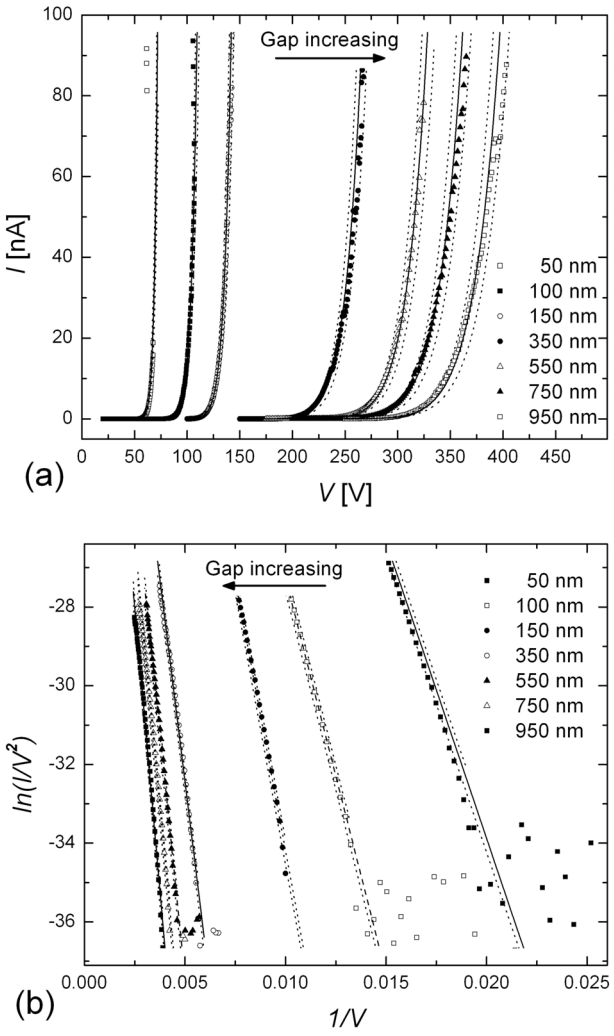

FIG. 3. Distance dependence of field emission in (a) I/V characteristics and (b) corresponding Fowler-Nordheim plots, measured for gaps from 50 to 950 nm between silicon AFM probe and TiW coated sample.

are also functions of the electric field, they induce the theoretical FN plot to be a slightly curved line. The small curvature results in a fitting error since we use a *linear* least-squares fitting method. Verification of this fitting model using artificial data learns that by using an iterative process, the parameters γ and A can be determined with errors of 2% for γ and 30% for A. This means that our fitting model is not fully self-consistent as has been found also by others[5,15] and should in principle be replaced by a nonlinear curve fitting method or local calculation for one point on the I-V characteristic. Although this causes a significant error in the values obtained for the area of emission, fortunately for the field enhancement factor this dependence is weak and γ can be fitted with sufficient accuracy for further analysis.

In Fig. 4 the field enhancement factors obtained from the FN plots are given as function of the probe-sample distance. As can be seen from the graph, the field enhancement factor is ~1 for small separation and increases with increasing distance. The model of Eq. (3) is used to fit the data points, by choosing values for r and γ_∞, giving a best fit for $\gamma_\infty=25$ and

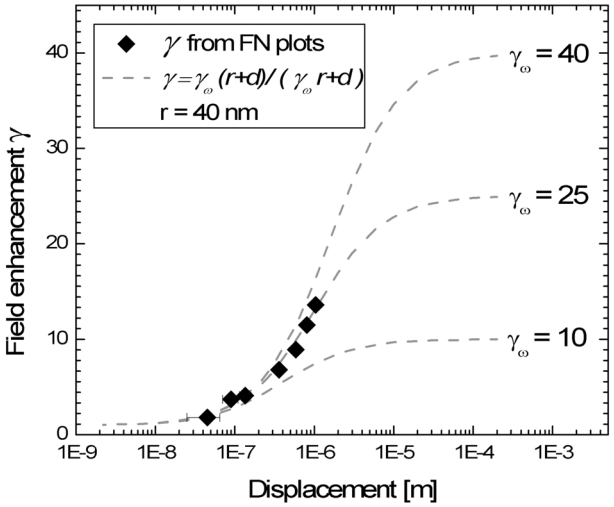

FIG. 4. Field enhancement factors determined by fitting the Fowler-Nordheim plots [Fig. 3(b)], plotted as function of electrode distance. Dashed lines are results of Eq. (3) with $r=40$ nm and $\gamma_\infty=10$, 25, and 40.

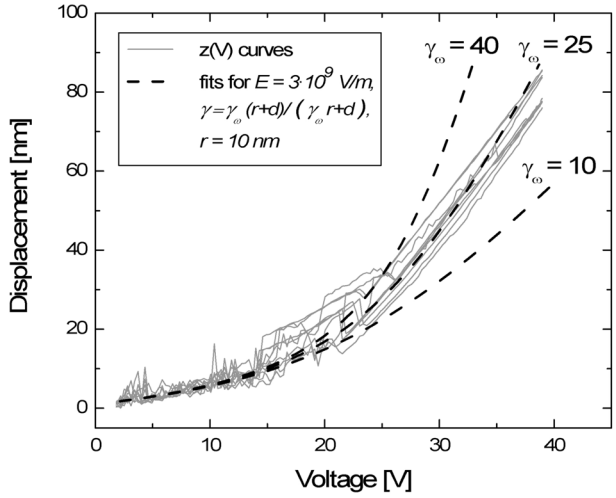

FIG. 5. Displacement measured as function of applied voltage (constant current 3 nA). Experiment repeated ten times. Fits determined by model from Eq. (3) using $r=10$ nm.

$r=40$ nm. This tip radius is larger than specified, which could be caused by slight damage to the AFM probe. Such damage has been observed by scanning electron microscopy on different probes, but unfortunately the measured probe could not be imaged due to failed unloading. The value for γ_∞ is lower than what is expected from Eq. (4) for an AFM tip length of 10 μm. The reason for this is probably that the pyramidal shape of the used probe tip is not well represented by the emitter sphere model used for the calculation of the field enhancement.

B. Control of probe-sample distance by constant current operation

By changing the bias voltage and keeping the field emission current constant using position feedback, the current signal can be used for position control. In Fig. 5 the relationship between the applied voltage and the probe position was measured by using feedback on the positioning actuator of the probe. When the applied voltage is increased from 5 to 40 V, the probe is retracted $\sim$90 nm in order to maintain a constant current of 3 nA. The accuracy of positioning during a single sweep was found to be within a few nanometers. However, for low voltages the sensitivity is less and was obscured by noise in the field emission current. At higher voltages, instabilities in the field emission current cause larger changes in the probe position and limit the positioning repeatability to $<$20 nm when repeating the experiment ten times.

The relation between displacement and voltage is fixed by the constant electric field at which field emission takes place. The nonlinearity of the curves can therefore be explained by a variation in the field enhancement factor. At low voltage, the probe is close to the sample and the field enhancement factor is $\sim$1. With increasing voltage the probe is retracted and the field enhancement increases, resulting in a larger slope. The measurement data were fitted using the model from Eq. (3) for an emission field of 3×10^9 V/m, which was determined from the measurements in Fig. 3. The best fit was obtained by using $r=10$ nm and $\gamma_\infty=25$. Note that this measurement is on a tip different from Fig. 4. For this smaller tip radius, typical for an undamaged AFM probe, the field enhancement reaches its maximum value at a shorter distance. The same value $\gamma_\infty=25$ as used in the fit of Fig. 4 was applied, which here determines the maximum slope of the curve at larger voltages.

C. Scanning on patterned samples using field emission currents for position feedback

The field emission displacement sensing method can be used for position feedback to keep the probe at several nanometers above a sample surface. By *scanning* the field emitter probe relative to a patterned sample, it is also possible to map the sample topography by recording the feedback signal.[2] To improve the current stability, the AFM probe was coated with 20 nm of chromium, changing the work function to $\phi=4.5$ eV.[14] Although there is a small change in work function, the distance dependence of the field emission current is not significantly affected for $\phi>4$ eV.[16]

Figure 6 shows the resulting scan images on a patterned sample using 3.0, 10.0, and 50.0 V bias voltage at 0.3 nA current setpoint. Increasing the bias voltage results in an increase in the probe-sample distance. Although a different probe is used than that characterized in Fig. 5, this distance variation is expected to be several tens of nanometers. The increase in distance is indicated by the loss of resolution between the sequential measurements. The noise level due to instabilities in the field emission current is large and increases with higher voltage, but the signal is sufficient to detect features of $\sim$20 nm. At small distance, a low scan rate (300 nm/s) was used to avoid probe-sample contacts. At larger distance higher scan speeds (4 μm/s) could be

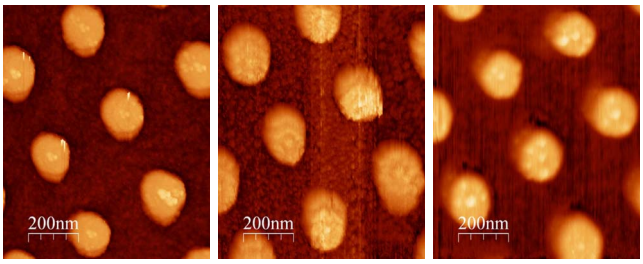

FIG. 6. Scanning an AFM probe coated with 20 nm Cr during position feedback (constant current 0.3 nA) results in a height image of the LILA sample. The bias voltage is increased from 3.0 V (left) to 10.0 V (middle) to 50.0 V (right) to increase the probe-sample distance.

used, which indicates that the probe-sample distance has increased beyond the height of the dots (~35 nm).

Scanning the samples using field emission for positioning should not alter the surface that is scanned. However, during initial measurements it was found that the field emission currents can cause significant damage to the sample surface. Two types of effects were observed. In Fig. 7, the top part of a 1.5×1.5 μm^2 scan is given that was measured at 3 V bias after scanning an area of 1×1 μm^2 in the center at 10 V bias. A surface profile of this measurement shows that the middle area is ablated with indentations up to 25 nm. We suppose that this ablation effect is the result of large current peaks, caused by instabilities in the field emission current or in the probe-sample distance.[17] By using a 100 MΩ resistor close to the field emitter probe, the effective capacitance of the tip is lowered and the ablation effect can be reduced.

The second damaging effect is shown in Fig. 8. Here part of a 1.5×1.5 μm^2 scan is given that was measured after scanning the center at 15 V bias. In this image the 1×1 μm^2 area in the middle of the image has a higher apparent topography (~5 nm) compared to the surrounding area. This is explained by deposition caused by field emitted electrons that dissociate adsorbed hydrocarbons on the sample surface.[18]

To further investigate this effect, an AFM measurement setup with interferometer deflection detection system was used. The AFM image in Fig. 9 shows the result after a single line trace on the sample surface, where in 30 s the bias voltage was ramped from 20 V down to 3 V and back. This resulted in material deposition with a linewidth of 100 nm and height up to ~70 nm. The deposition rate is high, since the electron beam energies at the used distances are close to the peak in the hydrocarbon dissociation cross section, with a threshold of ~10 eV.[19]

To prevent this field emission induced deposition, for all other measurements the field emitter probes and counter-electrode sample were annealed before use and operated in an UHV system that is frequently baked to maintain the necessary vacuum conditions.

V. CONCLUSIONS

In this paper we showed that the distance dependence of the field emission effect can be applied as a displacement sensing method and used to position an AFM probe with high resolution with respect to a patterned surface. A model based on finite element calculations was developed to calculate the sensitivity of the field emission current for small probe-sample distances. By measuring I/V characteristics for distances varying from 50 to 950 nm, the values for field enhancement factor were obtained from the corresponding FN plots and used to verify our model.

The probe-sample distance can be controlled up to 90 nm by operating the probes in constant current mode and varying the applied voltage. The nonlinearity in the measured voltage-displacement curve agrees with the same model for the distance dependence of the field enhancement. Although the positioning accuracy is still limited to ~20 nm by noise and instabilities in the emission current, the main outcome of this measurement is that the field emission current signal can indeed be used for position control.

Bias-dependent imaging can be used to scan on conducting patterned samples for increasing probe-sample distance.

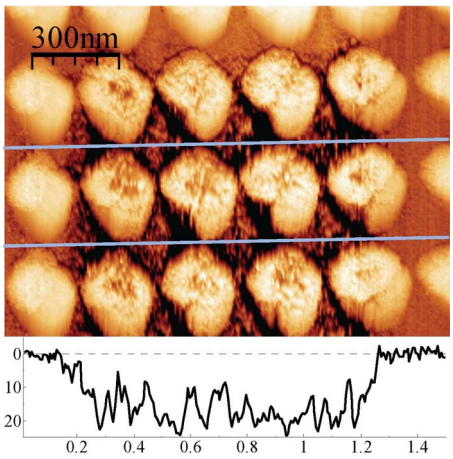

FIG. 7. Scan image (3 V, 3 nA) of the damage induced to the patterned sample by high field emission current peaks after scanning the center area at 10 V bias voltage.

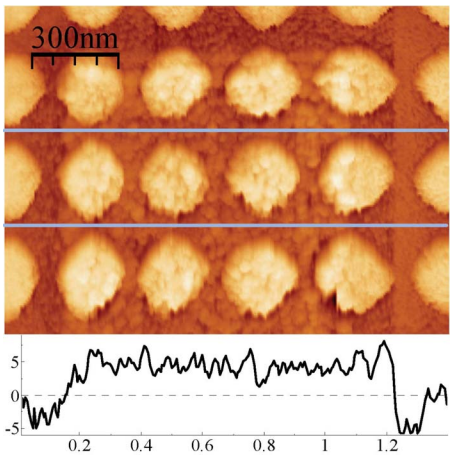

FIG. 8. Scan image (3 V, 3 nA) of the patterned sample, showing the field emission induced deposition after scanning the middle area at 15 V bias voltage.

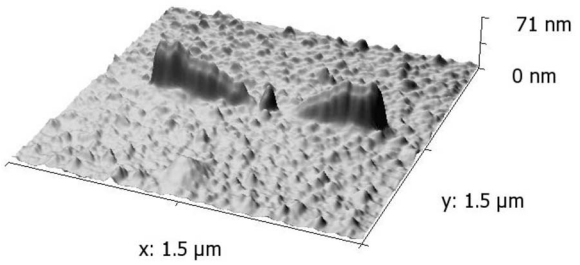

FIG. 9. AFM image of deposits induced by field emission currents. Lines were deposited by scanning the biased AFM probe in noncontact while ramping the voltage from 20 V down to 3 V and back.

At larger distances the lateral resolution reduces, but higher scan speeds can be used. Two damaging effects have to be prevented when using field emission currents during scanning: ablation of the surface due to large current peaks and field emission current induced deposition. These effects can be prevented by using a resistor close to the field emitter to limit the maximum emission currents and by annealing the probe and sample under UHV conditions before use.

The measurements confirm that field emission current can be applied to control the spacing between probe and medium, with sufficient resolution and current stability for probe storage applications. Since the sensitivity depends on the material work function, tip radius, and emitter geometry, very uniform emitters are required to prevent the need for individual calibration when using an array of probes. For practical applications, the field emission current stability should be improved to be sufficient also in poor vacuum conditions, which we try to achieve by using better field emitting materials.

ACKNOWLEDGMENTS

This work was funded by the Dutch Technology Foundation (STW) within the "Micro Scanning Probe Array Memory" project. The authors thank L. Bouwman for the data fitting procedure, R. Luttge for sample preparation, and M. Siekman for technical assistance.

[1] R. C. Smith, J. D. Carey, R. D. Forrest, and S. R. P. Silva, J. Vac. Sci. Technol. B **23**, 632 (2005).
[2] R. Young, J. Ward, and F. Scire, Rev. Sci. Instrum. **43**, 999 (1972).
[3] A. J. le Fèbre, R. Luttge, L. Abelmann, and J. C. Lodder, J. Phys.: Conf. Ser. **61**, 673 (2007).
[4] A. Knoll, P. Bächtold, J. Bonan, G. Cherubini, M. Despont, U. Drechsler, U. Dürig, B. Gotsmann, W. Häberle, C. Hagleitner *et al.*, Microlectron. Eng. **83**, 1692 (2006).
[5] R. G. Forbes, J. Vac. Sci. Technol. B **17**, 526 (1999).
[6] E. L. Murphy and R. H. Good, Phys. Rev. **102**, 1464 (1956).
[7] R. G. Forbes, C. J. Edgcombe, and U. Valdre, Ultramicroscopy **95**, 57 (2003).
[8] J. M. Bonard, M. Croci, I. Arfaoui, O. Noury, D. Sarangi, and A. Châtelain, Diamond Relat. Mater. **11**, 763 (2002).
[9] H. Kosmahl, IEEE Trans. Electron Devices **38**, 1534 (1991).
[10] H. Craig Miller, J. Appl. Phys. **38**, 4501 (1967).
[11] F. Hecht, O. Pironneau, and A. le Hyaric, *FreeFem++, a finite element PDE solver* (software version 2.14 from http://www.freefem.org, March 2007).
[12] M. W. Denhoff, J. Phys. D **39**, 1761 (2006).
[13] A. J. le Fèbre, M. Siekman, L. Abelmann, and J. C. Lodder, Transducers 2007 Solid-State Actuators and Microsystems Conference, 2007 (unpublished), p. 2361.
[14] W. Martienssen and H. Warlimont, *Handbook of Condensed Matter and Materials Data* (Springer, New York, 2005).
[15] R. G. Forbes, J. H. B. Deane, N. Hamid, and H. San Sim, J. Vac. Sci. Technol. B **22**, 1222 (2004).
[16] F. M. Charbonnier and E. E. Martin, J. Appl. Phys. **33**, 1897 (1962).
[17] P. G. Van Patten, J. D. Noll, M. L. Myrick, C. R. Li, and T. S. Sudarshan, J. Phys. Chem. **100**, 3646 (1996).
[18] M. A. McCord, D. P. Kern, and T. H. P. Chang, J. Vac. Sci. Technol. B **6**, 1877 (1988).
[19] D. A. Alman, D. N. Ruzic, and J. N. Brooks, Phys. Plasmas **7**, 1421 (2000).